

Article

Synthesis of Co₃O₄ Nanoplates by Thermal Decomposition for the Colorimetric Detection of Dopamine

Zengmin Tang ¹, Ling Zhang ¹, Sijia Tang ¹, Junping Li ², Jianxiong Xu ¹, Na Li ³ , Lijian Xu ¹ and Jingjing Du ^{4,*}

¹ Hunan Key Laboratory of Biomedical Nanomaterials and Devices, College of Life Sciences and Chemistry, Hunan University of Technology, Zhuzhou 412007, China

² Yichun Fangke Sewage Treatment Co., Ltd., Mingyue North Road 542, Yichun 336000, China

³ Hunan Key Laboratory of Electrochemical Green Metallurgy Technology, College of Materials and Advanced Manufacturing, Hunan University of Technology, Zhuzhou 412007, China

⁴ College of Packaging and Materials Engineering, Hunan University of Technology, Zhuzhou 412007, China

* Correspondence: dj19820923@126.com

Abstract: Inorganic nanomaterials with enzyme-like activity have been attracting much attention due to their low cost, favorable stability, convenient storage, and simple preparation. Herein, Co₃O₄ nanoplates with a uniform nanostructure were prepared by the thermolysis of cobalt hydroxide at different temperatures, and the influence of the annealing temperature on the performance of the mimetic enzyme also was reported for the first time. The results demonstrated that Co₃O₄ nanoplates obtained at an annealing temperature of 200 °C possessed strong oxidase activity and efficiently catalyzed the oxidation of 3,3',5,5'-tetramethylbenzidine (TMB) without the addition of hydrogen peroxide to generate the blue color product ox-TMB. Once the annealing temperature was increased to 500 °C and 800 °C, the oxidase activity of Co₃O₄ decreased rapidly, and was even inactivated. This might be attributed to the relatively large specific surface area of Co₃O₄ annealed at 200 °C. Besides this, based on the TMB-Co₃O₄ nanoplate system, a colorimetric analysis method was developed to detect dopamine with a limit of 0.82 μmol/L in a linear range from 1.6 μmol/L to 20 μmol/L.



Citation: Tang, Z.; Zhang, L.; Tang, S.; Li, J.; Xu, J.; Li, N.; Xu, L.; Du, J. Synthesis of Co₃O₄ Nanoplates by Thermal Decomposition for the Colorimetric Detection of Dopamine. *Nanomaterials* **2022**, *12*, 2990. <https://doi.org/10.3390/nano12172990>

Academic Editor: Alessandro Barge

Received: 5 August 2022

Accepted: 27 August 2022

Published: 29 August 2022

Publisher's Note: MDPI stays neutral with regard to jurisdictional claims in published maps and institutional affiliations.



Copyright: © 2022 by the authors. Licensee MDPI, Basel, Switzerland. This article is an open access article distributed under the terms and conditions of the Creative Commons Attribution (CC BY) license (<https://creativecommons.org/licenses/by/4.0/>).

Keywords: Co₃O₄; thermal decomposition; oxidase-like activity; colorimetric detection; dopamine

1. Introduction

Dopamine is a well-known considerable catecholamine neurotransmitter in the human central nervous, cardiovascular, and hormone systems [1]. A deficient level of dopamine may cause Parkinson's disease, and an excessive level of dopamine also may bring about abnormalities including schizophrenia and euphoria, etc. [2,3]. For the sake of convenience, it is necessary to develop point-of-care testing (POCT) for dopamine detection. The POCT system is an in vitro monitoring platform with a short turnout time; it can even can be operated by an unskilled user, which can promote the development of clinical testing and bring significant economic benefits [4]. Recently, various methods have been applied in POCT, such as fluorescence sensors, electrochemical methods, and colorimetric sensors [5–11].

In recent decades, electrochemical sensors to detect dopamine have received wide attention due to their facile operation and response [12–14]. However, the actual test experiments found that the research on the stability and reproducibility of the sensors still faces significant challenges. In addition, the recently developed colorimetric sensors based on oxidase-like nano-enzyme materials present a change in color and absorbance during the process of detecting dopamine, which also applies to the POCT system due to its low cost, simplicity, rapid measurement, and sensitive readout [15–17]. Compared with natural enzymes, nano-enzyme materials possess the advantage of high stability. The oxidase mimic can more effectively oxidize the colorless TMB into ox-TMB with a blue color in the absence of hydrogen peroxide [18]. The addition of dopamine can absorb the dissolved

oxygen or reactive oxygen, eventually leading to the fading of the color and the reduction of absorbance. Recently, precious metal nanomaterials have been considered as promising oxidase mimic candidates for application in colorimetric sensors [19], such as gold nanoparticles [20], platinum nanoparticles [21], silver nanoparticles [22], gold–platinum alloy nanoparticles [23], and silver–platinum alloy nanoparticles [24], etc. However, their high cost and limited resources inhibit their development and wide application. Therefore, transitional metal oxides performing comparable oxidase-like activity have also received considerable attention as a low-cost and available alternative [25–27].

As a transitional oxide, Co_3O_4 is an important p-type semiconductor with wide applications in supercapacitors, batteries, and catalysis, etc. [28–32]. In addition, Co_3O_4 nanoparticles also exhibit the behavior of mimic enzymes, and have received much attention for colorimetric sensors, enzyme-mimicking catalyzers, and so on [33,34]. In 2012, Mu et al. first reported Co_3O_4 with a catalase-like activity, which was applied to detect the concentration of H_2O_2 [35]. Shortly afterward, Qin et al., in 2014, found that the synthesized Co_3O_4 showed oxidase-like activity and could oxidize TMB to form colored ox-TMB, which has been applied for the detection of sulfite in food [36]. These results also demonstrated the great potential of Co_3O_4 for the detection of dopamine [37].

Two-dimensional nanoparticles are particles with one dimension that is limited to the nanometer scale; they have received wide attention due to their unique shape, anisotropic physical and chemical properties, and high surface-to-volume ratios [38]. In this study, the Co_3O_4 nanoplates were synthesized by the thermal decomposition of the as-prepared precursor $\text{Co}(\text{OH})_2$ at different temperatures for 30 min. The mimic enzyme behaviors of Co_3O_4 obtained at different annealing temperatures were discussed. The oxidase activity of Co_3O_4 was evaluated by Michaelis–Menten. Eventually, performances such as the sensitivity, selectivity, and lowest detection limit in the detection of dopamine were investigated.

2. Chemical and Methods

The cobalt chloride hexahydrate ($\text{CoCl}_2 \cdot 6\text{H}_2\text{O}$), glacial acetic acid (CH_3COOH), sodium acetate (CH_3COONa), branched polyethyleneimine solution (BPEI, Mw: 60,000, 50 wt% in water), octylamine ($\text{C}_8\text{H}_{19}\text{N}$), ethanol ($\text{C}_2\text{H}_5\text{OH}$), 3,3',5,5'-tetramethylbenzidine (TMB), potassium chloride (KCl), magnesium chloride (MgCl_2), ferric chloride (FeCl_3), and cupric sulfate (CuSO_4) were obtained from InnoChem science and technology Co. Ltd. (Beijing, China).

Regarding the fabrication of the Co_3O_4 nanoplates, Co_3O_4 nanoplates were prepared through two steps. First, $\text{Co}(\text{OH})_2$ was synthesized using the hydrothermal method, as described in the previous literature [39]. Briefly, 2 mmol CoCl_2 was added to 10 mL distilled water in the presence of 0.06 g BPEI, and was agitated constantly at 90 °C in a water bath. Then, the reaction was caused by adding 1 mL octylamine, and was maintained for around 40 min. After cooling, washing, and separation, the precursor $\text{Co}(\text{OH})_2$ was obtained. The second step was the decomposition of $\text{Co}(\text{OH})_2$ at different temperatures (200, 500, and 800 °C) for 30 min in a tube furnace in order to fabricate Co_3O_4 nanoplates. The samples synthesized at different calcination temperatures were named Co_3O_4 -200, Co_3O_4 -500, and Co_3O_4 -800.

Regarding the catalytic activity of the Co_3O_4 and kinetic analysis, briefly, 0.1 mL of various Co_3O_4 suspensions with a concentration of 3 mg/mL and 0.2 mL TMB with a concentration of 2 mmol/L were added to 2.7 mL CH_3COOH - CH_3COONa buffer solution (0.2 mol/L, pH = 4.0), and then the mixture was incubated at 40 °C for 30 min. In this system, the concentration of Co_3O_4 was 100 $\mu\text{g}/\text{mL}$, and the concentration of TMB was 133.3 $\mu\text{mol}/\text{L}$. Then, the ultraviolet–visible absorptions of the above solution between the range of 550–750 nm were recorded. The kinetic parameters were conducted at 40 °C using different concentrations of TMB whilst keeping the other conditions constant. Kinetic analysis was performed by recording the absorbance at 652 nm after incubation

for 30 min at 40 °C. The corresponding Michaelis–Menten constant was calculated by a Lineweaver–Burk plot [37]:

$$1/v = K_m/V_m (1/[C] + 1/K_m)$$

where K_m is the Michaelis–Menten constant, which is an indicator of Co_3O_4 -200's affinity for its TMB, $[C]$ is the concentration of TMB, v is the initial velocity, and V_m represents the maximal reaction velocity.

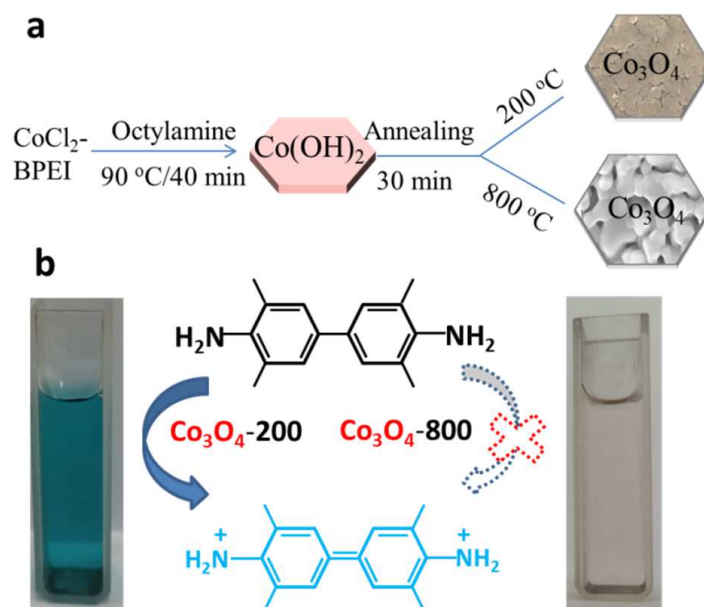
Regarding the colorimetric detection of dopamine, for the dopamine analysis, the absorption spectra of mixtures containing Co_3O_4 -200 (0.1 mL, 3 mg/mL), CH_3COOH – CH_3COONa buffer solution (2.7 mL, 0.2 mol/L), TMB (0.2 mL, 2 mmol/L), and dopamine with different concentrations from 1.6 to 20 $\mu\text{mol/L}$ were recorded from 550 to 750 nm. The change of absorbance ($\Delta A = A_0 - A$, where A_0 and A are the absorbances of the solution without and within the dopamine sample) at 652 nm versus the concentration of dopamine was applied to obtain the calibration curve. For the determination of the anti-interference performance, dopamine was detected in the presence of KCl, MgCl_2 , FeCl_3 , CuSO_4 , H_2O_2 , glucose, and urea with a concentration of 100 $\mu\text{mol/L}$.

Regarding the characterization, the morphology of the samples was characterized using a scanning electron microscope (SEM, Zeiss Gemini 300, Jena, Germany). The crystal structure was analyzed by X-ray diffraction (XRD, Bruker D8, Karlsruhe, Germany). The absorption spectrum in the range of 550–750 nm was measured using a UV-vis spectrophotometer (TU-1901). The surface area was detected by BET (Nova, Quantachrome, Boynton Beach, FL, USA).

3. Results and Discussion

3.1. Fabrication of Co_3O_4 Nanoplates

Based on the previous synthetic strategy [39], the pre-prepared $\text{Co}(\text{OH})_2$ nanoplates were first prepared and employed as the precursor to fabricate the Co_3O_4 nanoplates by regulating the annealing temperature. The thermal decomposition reaction only took 30 min at the designed temperature. The surface structure and oxidase-mimic activity of the Co_3O_4 nanoplates were significantly affected by the annealing temperature, as shown in Scheme 1.



Scheme 1. Schematic diagrams for (a) the synthetic pathway and (b) the oxidase performance of the Co_3O_4 nanoplates.

Powder XRD was used to characterize the crystal structure of the samples. Compared with the XRD pattern of $\text{Co}(\text{OH})_2$ (Figure 1a), the XRD pattern of Co_3O_4 -200 in Figure 1b changes with the intensity of the peaks and the new diffraction peaks. Several weak diffraction peaks at $2\theta = 19.0^\circ$, 31.3° , 36.8° , 44.8° , 59.3° , and 65.2° were assigned to the (111), (220), (311), (400), (511), and (440) crystal facets of cubic phase Co_3O_4 , respectively. Besides this, the crystal structures of the products are not affected by the higher calcination temperatures, such as 500°C and 800°C . Therefore, calcination at 200°C for 30 min can achieve the transformation of Co_3O_4 from $\text{Co}(\text{OH})_2$, which is 20 times shorter than the calcination time reported in the previous research [40].

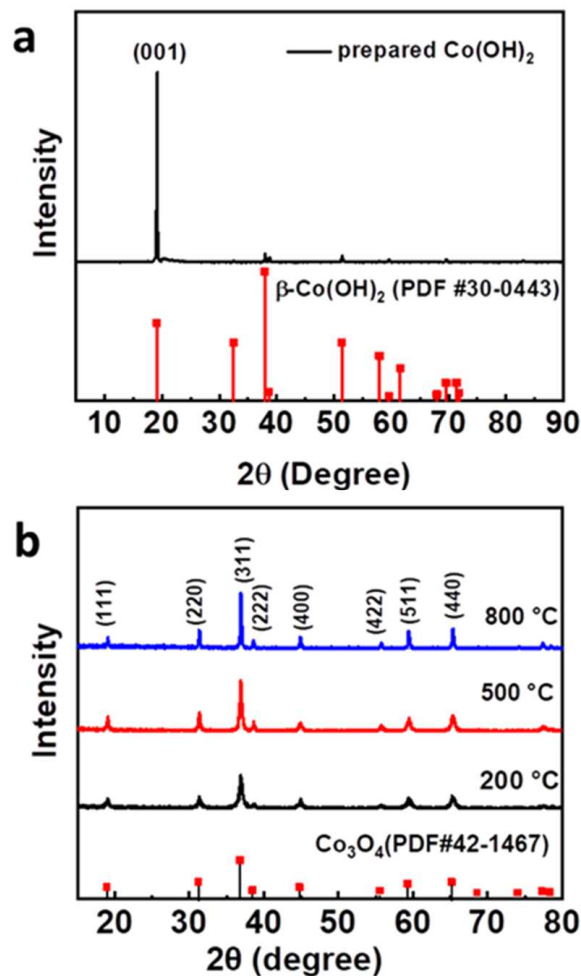


Figure 1. XRD patterns of (a) $\text{Co}(\text{OH})_2$ and (b) Co_3O_4 .

SEM was applied to observe the morphology of samples obtained at the different annealing temperatures. The SEM image in Figure 2a confirms that the precursor $\text{Co}(\text{OH})_2$ presents a hexagonal plate shape with a smooth surface, which is consistent with the previous study [39]. After the thermal decomposition of $\text{Co}(\text{OH})_2$ nanoplates at 200°C for 30 min, a black powder was obtained. As shown in the SEM image in Figure 2b, the obtained Co_3O_4 -200 remains in the shape of a hexagonal plate with a size range of 2–15 μm . Compared with $\text{Co}(\text{OH})_2$, cracks on the surface of the black samples can be observed due to the evaporation of water produced in the process of the thermal decomposition of $\text{Co}(\text{OH})_2$. In addition, the cracks are supposed to increase the surface area, and should eventually enhance the adsorption capacity and catalytic capacity. The surface structure of the samples hardly changed at the temperature of 500°C (Figure 2c). As the temperature increased to 800°C , pore structures were produced due to the fusion and recrystallization of the samples in the process at a high calcination temperature (Figure 2d).

As shown in Table 1, the Co_3O_4 -200 nanoplates have a relatively large specific surface area, which is 15 times greater than the specific surface area of the Co_3O_4 -500 and Co_3O_4 -800. The Co_3O_4 -800 presented a macropore structure, and the process of fusion and recrystallization would cause agglomeration, as shown in the insert SEM image in Figure 2d. In addition, the distribution of pore and pore size also was not uniform. Therefore, the sample Co_3O_4 -800 has a lower surface area according to the comprehensive analysis combined with agglomeration and uneven macropores.

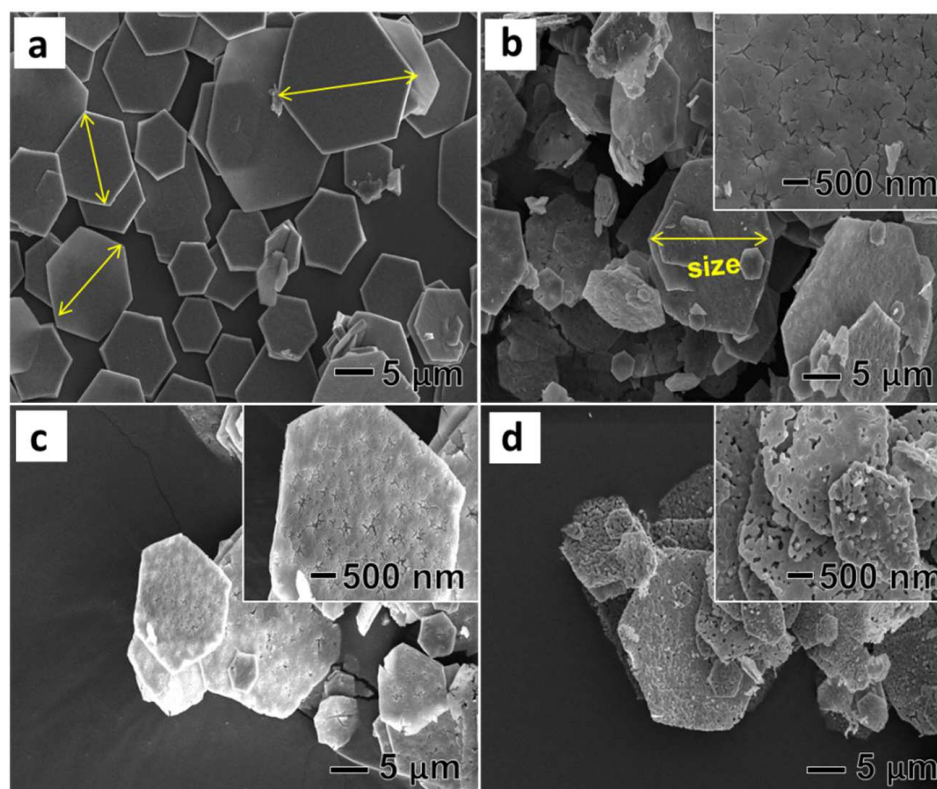


Figure 2. SEM image of samples including (a) $\text{Co}(\text{OH})_2$, (b) Co_3O_4 -200, (c) Co_3O_4 -500, and (d) Co_3O_4 -800.

Table 1. Specific surface area of the samples.

Samples	Specific Surface Area (m^2/g)
Co_3O_4 -200	80.472
Co_3O_4 -500	6.796
Co_3O_4 -800	5.158

3.2. Oxidase-like Activity of the Co_3O_4 Nanoplates

The oxidase-like activities of various types of Co_3O_4 were investigated by the catalytic oxidation of TMB in the absence of hydrogen peroxide, and the corresponding absorption at the range of wavelength from 550–750 nm was measured after incubation at 40 °C for 30 min. The results are shown in Figure 3a. Curve 1 demonstrates that the direct oxidation of TMB by dissolved oxygen in the absence of Co_3O_4 can be ignored. The obtained Co_3O_4 -200 nanoplates can catalyze the oxidation of colorless TMB to produce a blue product (ox-TMB), which has an obvious absorption peak at 652 nm (curve 4). On the contrary, the very weak absorption peaks in curve 2 and curve 3 reveal the sharply weakened oxidase enzyme behavior of the Co_3O_4 -500 and Co_3O_4 -800 nanoplates. Therefore, the oxidase activity of the obtained Co_3O_4 is seriously affected by the annealing temperature. In the process of catalysis, through adsorption for dissolved oxygen on the surface, the Co_3O_4

nanoplates are capable of catalyzing the dissolved oxygen to release reactive oxygen species accompanied by the oxidation of Co^{2+} to Co^{3+} [41]. In various reactive oxygen species, superoxide anions (O_2^-) acted as the main reactive oxygen species for the oxidation of TMB to blue ox-TMB. Due to its loose surface structure and larger surface area, Co_3O_4 -200 nanoplates can adsorb and catalyze more dissolved oxygen to release more superoxide anions, showing stronger catalytic activity for the oxidation of TMB. The curve in Figure 3b demonstrates that the oxidation of TMB catalyzed by Co_3O_4 -200 needs to take around 24 min to enter the steady state.

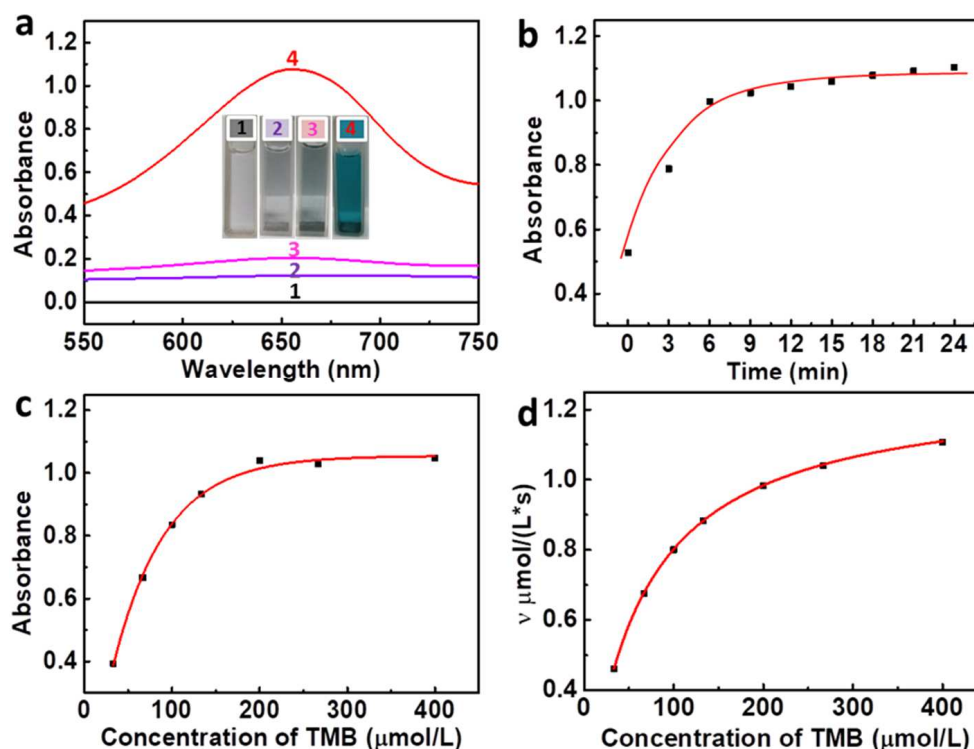


Figure 3. (a) Reaction between Co_3O_4 and TMB (curve 1-TMB + buffer, curve 2-TMB + buffer + Co_3O_4 -800, curve 3-TMB + buffer + Co_3O_4 -500, curve 4-TMB + buffer + Co_3O_4 -200), (b) the absorbance change of TMB in the presence of Co_3O_4 -200 over the time at 40 °C, (c) the absorbance change for different concentrations of TMB, and (d) the Michaelis–Menten curve of Co_3O_4 -200 with TMB.

In order to better understand the Co_3O_4 nanoplates' performance of an oxidase-like activity, the kinetic parameters of TMB alone were determined by varying the concentration of TMB, keeping the concentration of Co_3O_4 constant at 3 mg/mL. The absorbance change versus the concentration of TMB at 652 nm for 30 min is shown in Figure 3c. A typical Michaelis–Menten curve is shown in Figure 3d. The Michaelis–Menten constant (K_m) and maximum initial velocity (V_m) for the Co_3O_4 -200 nanoplate with TMB are 0.058 mmol/L and 1.27 μmol/(L*s), which are greater than the kinetic parameters reported for Co_3O_4 , $\text{Co}_3\text{O}_4/\text{CuO}$, and CoOOH [35,37,42]. It is suggested that synthesized Co_3O_4 -200 nanoplates possess a high affinity for TMB.

Additionally, the effects of temperature and pH on the oxidase-like activity of Co_3O_4 were explored. Firstly, the TMB- Co_3O_4 -200 suspension was incubated for 30 min at different temperatures while the pH was maintained at 4.0. The absorbance was recorded, and is shown in Figure 4a,b, which shows a similar absorbance in the range of 20 to 60 °C and a decrease of absorbance as the temperature increases to 70 °C. Then, the pH of the CH_3COOH - CH_3COONa buffer solution was controlled at 3.6, 4.0, 4.4, 4.8, and 5.2 as the temperature was kept at 40 °C. Figure 4c,d demonstrates that Co_3O_4 nanoplates possess a good oxidase-like activity at a pH of 3.6–4.4. The absorbance decreases once the pH

risers to 4.8 and 5.2. Therefore, the results illustrate that the Co_3O_4 can maintain a high oxidase-like activity in a wide temperature range from 20 to 60 °C with a pH of around 4.0.

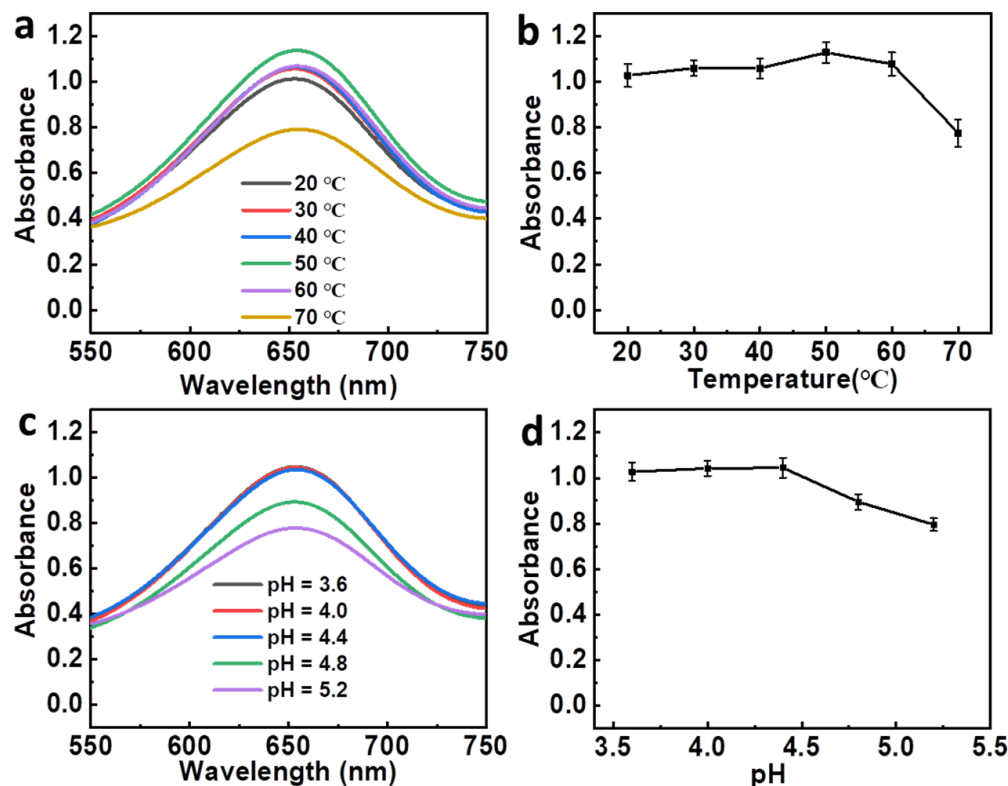


Figure 4. Effect of temperature (a,b) and pH (c,d) on the oxidase-like activity of Co_3O_4 -200.

3.3. Detection of Dopamine Employing the Co_3O_4 Nanoplates

As we found above, Co_3O_4 -200 can be used as an oxidase mimic, and can catalyze TMB to produce colored ox-TMB without the presence of hydrogen peroxide. In this research, in order to investigate the applicability of the oxidase-like Co_3O_4 -200, colorimetric detection for dopamine was conducted due to its inhibiting effect on the oxidase-like Co_3O_4 -200 nanoplates. Figure 5a shows that the blue color gradually fades with the increasing concentration of dopamine. Figure 5b further shows that the absorbance of the Co_3O_4 -TMB mixtures at 652 nm also gradually reduce with the increase of the dopamine concentration from 1.6 $\mu\text{mol/L}$ to 25 $\mu\text{mol/L}$, and a further increase in the concentration of dopamine only has a minor change in absorbance. The fading of the blue demonstrates that the oxidase-like mimic of Co_3O_4 -200 is inhibited by dopamine. This might be attributed to the fact that dopamine can induce the reduction of ox-TMB, or that dopamine more easily consumes the dissolved oxygen, which eventually leads to the decrease of the amounts of reactive oxygen species [43]. The corresponding ΔA versus the concentration of dopamine is shown in Figure 5c, which demonstrates that the concentration of detectible dopamine is around 1.6 $\mu\text{mol/L}$ in a linear range from 1.6 $\mu\text{mol/L}$ to 20 $\mu\text{mol/L}$. The limit of detection (LOD) for dopamine is as low as 0.82 $\mu\text{mol/L}$ ($S/N = 3$).

3.4. Analytic Performance for the Selectivity of Dopamine Detection

Selectivity is an important property of mimetic enzymes. Figure 6 shows the selectivity of oxidase Co_3O_4 -200 for dopamine detection in the presence of various substances, including K^+ , Mg^{2+} , Fe^{3+} , Cu^{2+} , Cl^- , SO_4^{2-} , H_2O_2 , glucose, and urea. The absorbance of the TMB-buffer- Co_3O_4 -200 system at 652 nm shows a significant decrease in the presence of 10 $\mu\text{mol/L}$ dopamine, while there are no significant changes in the absorbance for other substances with a concentration of 50 $\mu\text{mol/L}$. These results indicate that the oxidase Co_3O_4 -200 displays good selectivity for the detection of dopamine.

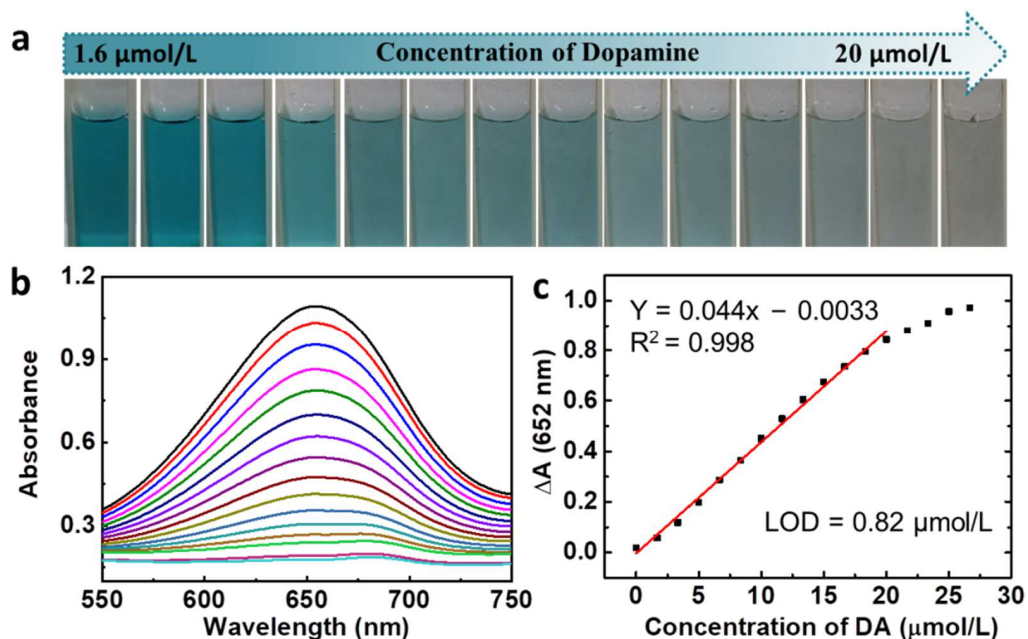


Figure 5. (a) Visual color changes of TMB-buffer- Co_3O_4 -200 with the increase of the concentration of dopamine, (b) the corresponding UV-vis absorption spectra, and (c) the plots of the net absorbance (ΔA) with the concentration of dopamine.

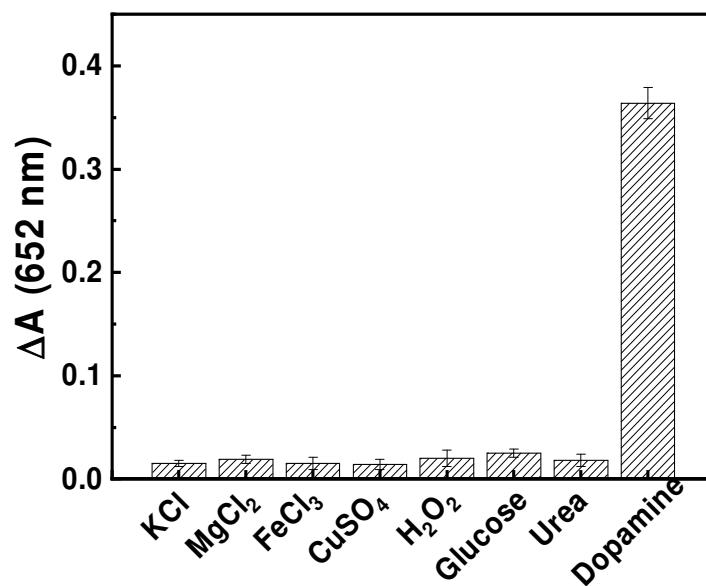


Figure 6. Change of ΔA in the presence of various substances.

4. Conclusions

Herein, Co_3O_4 nanoplates synthesized by thermal deposition possessed oxidase activity. The annealing temperature played an important role in tuning the oxidase activity of Co_3O_4 nanoplates. In these samples, Co_3O_4 nanoplates obtained at an annealing temperature of $200\text{ }^\circ\text{C}$ showed excellent oxidase activity due to their relatively large specific surface area and loose structure. As oxidase mimics, Co_3O_4 nanoplates were employed to develop a colorimetric sensor of dopamine with a limit of $0.82\text{ }\mu\text{mol/L}$ in a linear range from $1.6\text{ }\mu\text{mol/L}$ to $20\text{ }\mu\text{mol/L}$.

Author Contributions: Conceptualization, Z.T. and J.D.; Methodology, Z.T.; validation, Z.T., L.Z., S.T. and J.L.; formal analysis, J.X.; investigation, N.L.; resources, L.X.; data curation, Z.T.; writing—original draft preparation, Z.T.; writing—review and editing, L.X. and J.D.; project administration, L.X. and J.D. All authors have read and agreed to the published version of the manuscript.

Funding: Projects 51974116 and 51874128 were supported by the National Science Foundation of China; Projects 2020JJ4273 and 2020JJ5130 were supported by the Science Foundation of Hunan Province.

Institutional Review Board Statement: Not applicable.

Informed Consent Statement: Not applicable.

Data Availability Statement: Not applicable.

Conflicts of Interest: The authors declare no conflict of interest.

References

1. He, Q.; Liu, J.; Liu, X.; Li, G.; Deng, P.; Liang, J. Preparation of Cu₂O-reduced graphene nanocomposite modified electrodes towards ultrasensitive dopamine detection. *Sensors* **2018**, *18*, 199. [[CrossRef](#)] [[PubMed](#)]
2. Liu, X.; Liu, J. Biosensors and sensors for dopamine detection. *View* **2021**, *2*, 20200102. [[CrossRef](#)]
3. Gitler, A.D.; Dhillon, P.; Shorter, J. Neurodegenerative disease: Models, mechanisms, and a new hope. *Dis. Models Mech.* **2017**, *10*, 499–502. [[CrossRef](#)] [[PubMed](#)]
4. Yang, J.; Wang, K.; Xu, H.; Yan, W.; Jin, Q.; Cui, D. Detection platforms for point-of-care testing based on colorimetric, luminescent and magnetic assays: A review. *Talanta* **2019**, *202*, 96–110. [[CrossRef](#)] [[PubMed](#)]
5. He, Z.; Tong, Z.; Tan, B.; He, X.; Zhang, T.; Guo, Y.; Jin, L.; He, N.; Li, S.; Chen, Z. Rapid Detection of DNA Methylation with a Novel Real-Time Fluorescence Recombinase-Aided Amplification Assay. *J. Biomed. Nanotechnol.* **2021**, *17*, 1364–1370. [[CrossRef](#)]
6. Li, T.; Yi, H.; Liu, Y.; Wang, Z.; Liu, S.; He, N.; Liu, H.; Deng, Y. One-step synthesis of DNA templated water-soluble Au–Ag bimetallic nanoclusters for ratiometric fluorescence detection of DNA. *J. Biomed. Nanotechnol.* **2018**, *14*, 150–160. [[CrossRef](#)]
7. Yang, H.; Liu, M.; Jiang, H.; Zeng, Y.; Jin, L.; Luan, T.; Deng, Y.; He, N.; Zhang, G.; Zeng, X. Copy number variation analysis based on gold magnetic nanoparticles and fluorescence multiplex ligation-dependent probe amplification. *J. Biomed. Nanotechnol.* **2017**, *13*, 655–664. [[CrossRef](#)]
8. He, Q.; Liu, J.; Liu, X.; Li, G.; Chen, D.; Deng, P.; Liang, J. Fabrication of amine-modified magnetite-electrochemically reduced graphene oxide nanocomposite modified glassy carbon electrode for sensitive dopamine determination. *Nanomaterials* **2018**, *8*, 194. [[CrossRef](#)]
9. Liu, J.; Sun, L.; Li, G.; Hu, J.; He, Q. Ultrasensitive detection of dopamine via electrochemical route on spindle-like α -Fe₂O₃ Mesocrystals/rGO modified GCE. *Mater. Res. Bull.* **2021**, *133*, 111050. [[CrossRef](#)]
10. Li, F.; Ni, B.; Zheng, Y.; Huang, Y.; Li, G. A simple and efficient voltammetric sensor for dopamine determination based on ZnO nanorods/electro-reduced graphene oxide composite. *Surf. Interfaces* **2021**, *26*, 101375. [[CrossRef](#)]
11. Wu, Y.; Deng, P.; Tian, Y.; Feng, J.; Xiao, J.; Li, J.; Liu, J.; Li, G.; He, Q. Simultaneous and sensitive determination of ascorbic acid, dopamine and uric acid via an electrochemical sensor based on PVP-graphene composite. *J. Nanobiotechnol.* **2020**, *18*, 112. [[CrossRef](#)] [[PubMed](#)]
12. Li, G.; Zhong, P.; Ye, Y.; Wan, X.; Cai, Z.; Yang, S.; Xia, Y.; Li, Q.; Liu, J.; He, Q. A highly sensitive and stable dopamine sensor using shuttle-like α -Fe₂O₃ nanoparticles/electro-reduced graphene oxide composites. *J. Electrochem. Soc.* **2019**, *166*, B1552. [[CrossRef](#)]
13. He, Q.; Liu, J.; Liu, X.; Li, G.; Chen, D.; Deng, P.; Liang, J. A promising sensing platform toward dopamine using MnO₂ nanowires/electro-reduced graphene oxide composites. *Electrochim. Acta* **2019**, *296*, 683–692. [[CrossRef](#)]
14. Liu, H.; Xiong, R.; Zhong, P.; Li, G.; Liu, J.; Wu, J.; Liu, Y.; He, Q. Nanohybrids of shuttle-like α -Fe₂O₃ nanoparticles and nitrogen-doped graphene for simultaneous voltammetric detection of dopamine and uric acid. *New J. Chem.* **2020**, *44*, 20797–20805. [[CrossRef](#)]
15. Liu, X.; He, F.; Zhang, F.; Zhang, Z.; Huang, Z.; Liu, J. Dopamine and melamine binding to gold nanoparticles dominates their aptamer-based label-free colorimetric sensing. *Anal. Chem.* **2020**, *92*, 9370–9378. [[CrossRef](#)]
16. Chen, Q.; Liang, C.; Zhang, X.; Huang, Y. High oxidase-mimic activity of Fe nanoparticles embedded in an N-rich porous carbon and their application for sensing of dopamine. *Talanta* **2018**, *182*, 476–483. [[CrossRef](#)]
17. Liang, L.; Zhao, Z.; Ye, F.; Zhao, S. Rapid and sensitive colorimetric detection of dopamine based on the enhanced-oxidase mimicking activity of cerium (IV). *New J. Chem.* **2021**, *45*, 6780–6786. [[CrossRef](#)]
18. Wang, H.; Wan, K.; Shi, X. Recent advances in nanozyme research. *Adv. Mater.* **2019**, *31*, 1805368. [[CrossRef](#)]
19. Chen, W.; Li, S.; Wang, J.; Sun, K.; Si, Y. Metal and metal-oxide nanozymes: Bioenzymatic characteristics, catalytic mechanism, and eco-environmental applications. *Nanoscale* **2019**, *11*, 15783–15793. [[CrossRef](#)]
20. Lou-Franco, J.; Das, B.; Elliott, C.; Cao, C. Gold nanozymes: From concept to biomedical applications. *Nano-Micro Lett.* **2021**, *13*, 10. [[CrossRef](#)]

21. Deng, H.; He, S.; Lin, X.; Yang, L.; Lin, Z.; Chen, R. Target-triggered inhibiting oxidase-mimicking activity of platinum nanoparticles for ultrasensitive colorimetric detection of silver ion. *Chin. Chem. Lett.* **2019**, *30*, 1659–1662. [[CrossRef](#)]
22. Xu, D.; Li, R.; Wang, Q.; Yang, Y.; Wang, G.; Li, Z. Synthesis of silver nanocrystal with an excellent oxidase-like activity and its application in colorimetric detection of D-penicillamine. *Microchem. J.* **2021**, *166*, 106204.
23. Chi, H.; Cui, X.; Lu, Y.; Yu, M.; Fei, Q.; Feng, G. Colorimetric determination of cysteine based on Au@Pt nanoparticles as oxidase mimetics with enhanced selectivity. *Microchim. Acta* **2022**, *189*, 13. [[CrossRef](#)] [[PubMed](#)]
24. Cai, S.; Jia, X.; Han, Q.; Yan, X.; Yang, R.; Wang, C. Porous Pt/Ag nanoparticles with excellent multifunctional enzyme mimic activities and antibacterial effects. *Nano Res.* **2017**, *10*, 2056–2069. [[CrossRef](#)]
25. Chen, Z.J.; Huang, Z.; Sun, Y.M.; Xu, Z.L.; Liu, J. The most active oxidase-mimicking Mn₂O₃ nanozyme for biosensor signal generation. *Chem. Eur. J.* **2021**, *27*, 9597–9604. [[CrossRef](#)]
26. Wang, X.; Feng, S.; He, D.; Jiang, P. Porous manganese–cobalt oxide microspheres with tunable oxidase mimicking activity for sulfide ion colorimetric detection. *Chem. Commun.* **2020**, *56*, 14098–14101. [[CrossRef](#)]
27. Huang, L.; Zhang, W.; Chen, K.; Zhu, W.; Liu, X.; Wang, R.; Zhang, X.; Hu, N.; Suo, Y.; Wang, J. Facet-selective response of trigger molecule to CeO₂{110} for up-regulating oxidase-like activity. *Chem. Eng. J.* **2017**, *330*, 746–752. [[CrossRef](#)]
28. Lu, Y.; Liu, Y.; Mo, J.; Deng, B.; Wang, J.; Zhu, Y.; Xiao, X.; Xu, G. Construction of hierarchical structure of Co₃O₄ electrode based on electrospinning technique for supercapacitor. *J. Alloys Compd.* **2021**, *853*, 157271. [[CrossRef](#)]
29. Li, N.; Yuan, K.; Gao, T.; Li, S.; Qin, J.; Zhu, Y.; Du, J.; Xu, J. Controllable synthesis of hierarchical nanoporous carbon@Ni(OH)₂ rambutan-like composite microspheres for high-performance hybrid supercapacitor. *Arab. J. Chem.* **2022**, *15*, 103580. [[CrossRef](#)]
30. Cordeiro, P.V.O.; Carvalho, N.M. Water oxidation reaction catalyzed by Co₃O₄ treated with organic compounds. *Ind. Eng. Chem. Res.* **2018**, *57*, 11259–11264. [[CrossRef](#)]
31. Yi, C.; Zou, J.; Yang, H.; Leng, X. A facile hydrothermal synthesis of graphene/RuO₂/Co₃O₄ nanocomposites with high pseudocapacity. *New J. Chem.* **2018**, *42*, 7066–7072. [[CrossRef](#)]
32. Zhang, J.; Feng, J.; Tian, Y.; Wu, Y.; Liu, X.; He, Q. Ultrasensitive electrochemical determination of tyrosine based on the α-Fe₂O₃@Co₃O₄-NRGO modified electrode. *Microchem. J.* **2021**, *171*, 106867. [[CrossRef](#)]
33. Wang, T.; Su, P.; Li, H.; Yang, Y.; Yang, Y. Triple-enzyme mimetic activity of Co₃O₄ nanotubes and their applications in colorimetric sensing of glutathione. *New J. Chem.* **2016**, *40*, 10056–10063. [[CrossRef](#)]
34. Liu, X.; Yan, L.; Ren, H.; Cai, Y.; Liu, C.; Zeng, L.; Guo, J.; Liu, A. Facile synthesis of magnetic hierarchical flower-like Co₃O₄ spheres: Mechanism, excellent tetra-enzyme mimics and their colorimetric biosensing applications. *Biosens. Bioelectron.* **2020**, *165*, 112342. [[CrossRef](#)]
35. Mu, J.; Wang, Y.; Zhao, M.; Zhang, L. Intrinsic peroxidase-like activity and catalase-like activity of Co₃O₄ nanoparticles. *Chem. Commun.* **2012**, *48*, 2540–2542. [[CrossRef](#)] [[PubMed](#)]
36. Qin, W.; Su, L.; Yang, C.; Ma, Y.; Zhang, H.; Chen, X. Colorimetric detection of sulfite in foods by a TMB–O₂–Co₃O₄ nanoparticles detection system. *J. Agric. Food Chem.* **2014**, *62*, 5827–5834. [[CrossRef](#)] [[PubMed](#)]
37. Zhuang, Y.; Zhang, X.; Chen, Q.; Li, S.; Cao, H.; Huang, Y. Co₃O₄/CuO hollow nanocage hybrids with high oxidase-like activity for biosensing of dopamine. *Mater. Sci. Eng. C* **2019**, *94*, 858–866. [[CrossRef](#)]
38. Chimene, D.; Alge, D.L.; Gaharwar, A.K. Two-Dimensional Nanomaterials for Biomedical Applications: Emerging Trends and Future Prospects. *Adv. Mater.* **2015**, *27*, 7261–7284. [[CrossRef](#)]
39. Wen, P.; Huang, J.; Kang, M.; Chen, S.; Xu, L.; Tang, Z. A facile synthesis of cobalt hydroxide nanoplates and electrochemical performance in supercapacitor application. *Mater. Express* **2021**, *11*, 551–556.
40. Xu, L.; Zhang, L.; Tang, S.; Tang, Z. Preparation of Co₃O₄ and Its Application in Electrochemical Detection of H₂O₂. *Packaging J.* **2022**, *14*, 1–8.
41. Zhao, Q.; Zheng, X.Y.; Xing, L.; Tang, Y.L.; Zhou, X.M.; Hu, L.; Yao, W.L.; Yan, Z.Q. 2D Co₃O₄ stabilizing Rh nano composites developed for visual sensing bioactive urea and toxic p-aminophenol in practice by synergetic-reinforcing oxidase activity. *J. Hazard. Mater.* **2021**, *409*, 125019. [[CrossRef](#)] [[PubMed](#)]
42. Wang, Y.M.; Liu, J.W.; Jiang, J.H.; Zhong, W. Cobalt oxyhydroxide nanoflakes with intrinsic peroxidase catalytic activity and their application to serum glucose detection. *Anal. Bioanal. Chem.* **2017**, *409*, 4225–4232. [[CrossRef](#)] [[PubMed](#)]
43. Darbin, O. The aging striatal dopamine function. *Parkinsonism Relat. Disord.* **2012**, *18*, 426–432. [[CrossRef](#)] [[PubMed](#)]